Ultra-compact fiber-optic two-photon microscope for functional fluorescence imaging *in vivo*

Christoph J. Engelbrecht[1], Richard S. Johnston[2], Eric J. Seibel[2], Fritjof Helmchen[1,*]

1) Dept. of Neurophysiology, Brain Research Institute, University of Zurich,
Winterthurerstrasse 190, CH-8057 Zurich, Switzerland
2) Dept. of Mechanical Engineering and Human Photonics Laboratory, Fluke Hall,
University of Washington, Seattle, WA, USA
*Corresponding author: helmchen@hifo.uzh.ch

Abstract: We present a small, lightweight two-photon fiberscope and demonstrate its suitability for functional imaging in the intact brain. Our device consists of a hollow-core photonic crystal fiber for efficient delivery of near-IR femtosecond laser pulses, a spiral fiber-scanner for resonant beam steering, and a gradient-index lens system for fluorescence excitation, dichroic beam splitting, and signal collection. Fluorescence light is remotely detected using a standard photomultiplier tube. All optical components have 1 mm dimensions and the microscope's headpiece weighs only 0.6 grams. The instrument achieves micrometer resolution at frame rates of typically 25 Hz with a field-of-view of up to 200 microns. We demonstrate functional imaging of calcium signals in Purkinje cell dendrites in the cerebellum of anesthetized rats. The microscope will be easily portable by a rat or mouse and thus should enable functional imaging in freely behaving animals.

References and links

1. E. Seibel, T. Soper, R. Johnston, and R. Glenny, "Ultrathin laser scanning bronchoscope and guidance system for the peripheral lung," Lung Cancer **49**, S162-S162 (2005).
2. E. J. Seibel, R. S. Johnston, C. M. Brown, J. A. Dominitz, and M. B. Kimmey, "Novel ultrathin scanning fiber endoscope for cholangioscopy and pancreatoscopy," Gastrointest. Endosc. **65**, Ab125-Ab125 (2007).
3. A. F. Low, G. J. Tearney, B. E. Bouma, and I. K. Jang, "Technology insight: optical coherence tomography - current status and future development," Nature Clinical Practice Cardiovascular Medicine **3**, 154-162 (2006).
4. Z. Yaqoob, J. G. Wu, E. J. McDowell, X. Heng, and C. H. Yang, "Methods and application areas of endoscopic optical coherence tomography," J. Biomed. Opt. **11**, 063001 (2006).
5. F. Helmchen, "Miniaturization of fluorescence microscopes using fibre optics," Exp. Physiol. **87**, 737-745 (2002).
6. A. D. Mehta, J. C. Jung, B. A. Flusberg, and M. J. Schnitzer, "Fiber optic in vivo imaging in the mammalian nervous system," Curr. Opin. Neurobiol. **14**, 617-628 (2004).
7. B. A. Flusberg, E. D. Cocker, W. Piyawattanametha, J. C. Jung, E. L. M. Cheung, and M. J. Schnitzer, "Fiber-optic fluorescence imaging," Nature Methods **2**, 941-950 (2005).
8. L. Fu and M. Gu, "Fibre-optic nonlinear optical microscopy and endoscopy," J. Microsc. **226**, 195-206 (2007).
9. J. C. Jung, A. D. Mehta, E. Aksay, R. Stepnoski, and M. J. Schnitzer, "In vivo mammalian brain Imaging using one- and two-photon fluorescence microendoscopy," J. Neurophysiol. **92**, 3121-3133 (2004).
10. M. J. Levene, D. A. Dombeck, K. A. Kasischke, R. P. Molloy, and W. W. Webb, "In vivo multiphoton microscopy of deep brain tissue," J. Neurophysiol. **91**, 1908-1912 (2004).

11. F. Helmchen, M. S. Fee, D. W. Tank, and W. Denk, "A miniature head-mounted two-photon microscope: High-resolution brain imaging in freely moving animals," Neuron **31**, 903-912 (2001).
12. H. Adelsberger, O. Garaschuk, and A. Konnerth, "Cortical calcium waves in resting newborn mice," Nat. Neurosci. **8**, 988-990 (2005).
13. M. Murayama, E. Perez-Garci, H. R. Luscher, and M. E. Larkum, "Fiberoptic system for recording dendritic calcium signals in layer 5 neocortical pyramidal cells in freely moving rats," J. Neurophysiol. **98**, 1791-1805 (2007).
14. W. Denk, J. H. Strickler, and W. W. Webb, "Two-Photon Laser Scanning Fluorescence Microscopy," Science **248**, 73-76 (1990).
15. W. Denk and K. Svoboda, "Photon upmanship: why multiphoton imaging is more than a gimmick," Neuron **18**, 351-357 (1997).
16. F. Helmchen and W. Denk, "Deep tissue two-photon microscopy," Nature Methods **2**, 932-940 (2005).
17. J. Knittel, L. Schnieder, G. Buess, B. Messerschmidt, and T. Possner, "Endoscope-compatible confocal microscope using a gradient index-lens system," Opt. Commun. **188**, 267-273 (2001).
18. J. C. Jung and M. J. Schnitzer, "Multiphoton endoscopy," Opt. Lett. **28**, 902-904 (2003).
19. W. Göbel, J. N. D. Kerr, A. Nimmerjahn, and F. Helmchen, "Miniaturized two-photon microscope based on a flexible coherent fiber bundle and a gradient-index lens objective," Opt. Lett. **29**, 2521-2523 (2004).
20. D. G. Ouzounov, K. D. Moll, M. A. Foster, W. R. Zipfel, W. W. Webb, and A. L. Gaeta, "Delivery of nanojoule femtosecond pulses through large-core microstructured fibers," Opt. Lett. **27**, 1513-1515 (2002).
21. F. Helmchen, D. W. Tank, and W. Denk, "Enhanced two-photon excitation through optical fiber by single-mode propagation in a large core," Appl. Opt. **41**, 2930-2934 (2002).
22. W. Göbel, A. Nimmerjahn, and F. Helmchen, "Distortion-free delivery of nanojoule femtosecond pulses from a Ti : sapphire laser through a hollow-core photonic crystal fiber," Opt. Lett. **29**, 1285-1287 (2004).
23. B. A. Flusberg, J. C. Lung, E. D. Cocker, E. P. Anderson, and M. J. Schnitzer, "In vivo brain imaging using a portable 3.9 gram two-photon fluorescence microendoscope," Opt. Lett. **30**, 2272-2274 (2005).
24. M. T. Myaing, D. J. MacDonald, and X. D. Li, "Fiber-optic scanning two-photon fluorescence endoscope," Opt. Lett. **31**, 1076-1078 (2006).
25. L. Fu, X. Gan, and M. Gu, "Nonlinear optical microscopy based on double-clad photonic crystal fibers," Opt. Express **13**, 5528-5534 (2005).
26. J. Sawinski and W. Denk, "Miniature random-access fiber scanner for in vivo multiphoton imaging," J. Appl. Phys. **102**, (2007).
27. W. Piyawattanametha, R. P. J. Barretto, T. H. Ko, B. A. Flusberg, E. D. Cocker, H. J. Ra, D. S. Lee, O. Solgaard, and M. J. Schnitzer, "Fast-scanning two-photon fluorescence imaging based on a microelectromechanical systems two-dimensional scanning mirror," Opt. Lett. **31**, 2018-2020 (2006).
28. L. Fu, A. Jain, H. Xie, C. Cranfield, and M. Gu, "Nonlinear optical endoscopy based on a double-clad photonic crystal fiber and a MEMS mirror," Opt. Express **14**, 1027-1032 (2006).
29. A. Monfared, N. H. Blevins, E. L. M. Cheung, J. C. Jung, G. Popelka, and M. J. Schnitzer, "In vivo Imaging of mammalian cochlear blood flow using fluorescence microendoscopy," Otology & Neurotology **27**, 144-152 (2006).
30. P. Vincent, U. Maskos, I. Charvet, L. Bourgeais, L. Stoppini, N. Leresche, J. P. Changeux, R. Lambert, P. Meda, and D. Paupardin-Tritsch, "Live imaging of neural structure and function by fibred fluorescence microscopy," EMBO Rep **7**, 1154-1161 (2006).
31. E. J. Seibel and Q. Y. J. Smithwick, "Unique features of optical scanning, single fiber endoscopy," Lasers Surg. Med. **30**, 177-183 (2002).
32. E. J. Seibel, R. S. Johnston, and C. D. Melville, "A full-color scanning fiber endoscope," Optical Fibers and Sensors for Medical Diagnostics and Treatment Applications VI. Proceedings of the SPIE. **6083**, 9-16 (2006).
33. S. W. Grill and E. H. K. Stelzer, "Method to calculate lateral and axial gain factors of optical setups with a large solid angle," J. Opt. Soc. Am. A **16**, 2658-2665 (1999).
34. C. J. Engelbrecht and E. H. K. Stelzer, "Resolution enhancement in a light-sheet-based microscope (SPIM)," Opt. Lett. **31**, 1477-1479 (2006).
35. M. R. Sullivan, A. Nimmerjahn, D. V. Sarkisov, F. Helmchen, and S. S. Wang, "In vivo calcium imaging of circuit activity in cerebellar cortex," J. Neurophysiol. **94**, 1636-1644 (2005).
36. C. Stosiek, O. Garaschuk, K. Holthoff, and A. Konnerth, "In vivo two-photon calcium imaging of neuronal networks," Proc. Natl. Acad. Sci. U S A **100**, 7319-7324 (2003).
37. W. Göbel and F. Helmchen, "New angles on neuronal dendrites in vivo," J. Neurophysiol. **98**, 3770-3779 (2007).
38. J.-F. Cardoso, "BLIND SOURCE SEPARATION and INDEPENDENT COMPONENT ANALYSIS," http://www.tsi.enst.fr/~cardoso/guidesepsou.html.
39. D. A. Dombeck, A. N. Khabbaz, F. Collman, T. L. Adelman, and D. W. Tank, "Imaging large-scale neural activity with cellular resolution in awake, mobile mice," Neuron **56**, 43-57 (2007).

1. Introduction

Advances in the development of miniaturized fiber-optic imaging devices are opening new avenues for biomedical research and clinical imaging. For example, flexible catheter-like probes for video endoscopy [1, 2] or optical coherence tomography [3, 4] enable minimally invasive medical imaging, diagnosis, and potential treatment. While some applications rely on large field-of-views (FOV), others require a high spatial resolution in order to resolve cellular structures. Various approaches have been explored to build miniature high-resolution microscopes, including the design of microendoscopes, miniature confocal laser-scanning microscopes, coherent fiber-bundle imagers and nonlinear fluorescence microscopes (reviewed in [5-8]). Besides their potential impact for clinical applications, fiber-optic devices have great promises as new tools in neuroscientific research. In combination with fluorescent dyes for optical probing of neural activity and miniature gradient-index (GRIN) lens designs, they may allow *in vivo* endoscopic imaging of cells in deep brain structures [9, 10] as well as functional imaging of cellular activities in freely behaving animals [11-13].

Two-photon microscopy [14] is especially well suited for imaging deep inside biological tissue [15, 16]. Therefore miniaturization of two-photon microscopes has gained particular interest. Following the first demonstration of a fiber-optic two-photon microscope [11] various instruments of decreasing size have been presented. Key technological achievements have been the application of micro-optical components such as GRIN lenses [17-19], the use of special optical fibers for efficient laser pulse delivery [20-23] and fluorescence collection [24, 25], respectively, and the development of compact laser scanning devices. Two scanning methods have prevailed: (1) mechanical deflection or vibration of fiber cantilevers [11, 23, 26], and (2) microelectromechanical systems (MEMS) with small mirrors [27, 28]. Alternatively, a coherent fiber bundle can circumvent the need for scanning at the microscope headpiece albeit at the cost of reduced spatial resolution and sensitivity [19]. Despite these technical advances, only few functional measurements have been demonstrated with miniature fiberscopes, possibly because of the challenges in terms of sensitivity and stability. Functional studies comprise blood flow measurements in rodent brain [11] and cochlea [29] and measurements of neuronal activity using fluorescent calcium indicators in anesthetized animals [11, 30]. So far, calcium imaging in awake, freely moving animals has only been achieved using fiber-optic approaches with low or no spatial resolution [12, 13]. A routine application of fiber-optic microscopes for spatially-resolved functional imaging in awake animals is still pending.

Here we present a novel ultra-compact design of a two-photon fiberscope combining a miniature fiber scanner originally developed for video endoscopy [31] with optical and fiber components suitable for two-photon excited fluorescence measurements. We provide an optical characterization of our instrument and we demonstrate *in vivo* calcium imaging of dendritic activity in Purkinje cells of rat cerebellum.

2. Methods and results

2.1 Optical setup and fiberscope design

Near-infrared laser pulses (λ = 812 nm, $\tau \approx$ 100 fs) generated by an ultrafast Ti:Sapphire laser system (Tsunami and Millenia-X, Spectra-Physics, CA) were intensity modulated by a Pockels cell (Conoptics Inc., CT) and coupled into a hollow-core photonic crystal fiber (PCF, HC-800-01/-02, Crystal Fibre A/S, Birkerod, Denmark) for efficient pulse delivery with minimal distortions [22]. The laser beam was expanded and collimated with two telescopes (concave mirror pairs with focal lengths f_1=50 mm and f_2=100 mm, respectively). It was coupled to the PCF with a f =18.4 mm aspheric lens (Geltech) matching the numerical aperture (NA) of the PCF for maximum coupling efficiency. We achieved 30-40% transmission through the fiber with maximum average laser power levels of ~300 mW at the sample.

Laser pulses were guided through the PCF to the ultra-compact fiberscope headpiece (Fig. 1(a) and (b)). We used an ultra-thin spiral-pattern fiber scanner, which is based on a recently

developed micro-endoscope system [2, 31, 32]. Resonant vibrations (resonance frequency $v \approx$ 5 kHz; quality factor $Q \approx 50$) were induced in a fiber cantilever of about 4.5-mm length by using a custom-designed tubular piezoelectric actuator equipped with quadrant electrodes. Application of drive signals to the piezo tube with a phase shift of $\phi = 90°$ between x- and y-direction induced cyclic spiral motions of the fiber cantilever (Fig. 1(c) and (d)). Appropriate amplitude modulation was used to create a spiral scan pattern (using linear or sinusoidal segments as envelopes) [24, 32]. Specifically, expanding outward spirals were used for the imaging portion. Each imaging period was followed by shorter periods of retrace and fiber settling. The durations of the three phases could be arbitrarily chosen. To create 128x128–512x512 pixel images we used 64–520 expanding spiral cycles, typically 25 cycles for retracing and 50-100 cycles as settling period. These parameters result in frame rates of 36–8 frames per second (fps). In the *in vivo* experiments, we typically used scanning cycles near video rate (25 Hz), producing 128x128 pixel images with 80-130 expanding spirals, 25 retrace spirals, and 50-100 settling spirals. Optional online averaging could be used to efficiently reduce noise at the cost of lowering the frame rates.

The spiral motion of the fiber cantilever was imaged to the sample plane by a custom-designed assembly of GRIN-lenses with 1-mm diameter and dichroic beam-splitting 1-mm prisms (GRINTECH GmbH, Jena, Germany). The dichroic coating was designed to reflect ~93% of the near-IR excitation light while transmitting ~95% of the fluorescence emission light in the visible regime (~530 nm). Both values are for mixed s- and p-polarized light. The back lens served as a tube lens (working distance 450 μm in air) and had a maximum NA of 0.2. The front objective lens (maximum NA=0.5) had a working distance of 300 μm in water, thus yielding a demagnification factor of 2.5x. The FOV in the sample plane was determined by the maximal fiber deflection and the lens demagnification factor. With our instrument, we achieved FOVs of up to 200 μm in diameter. Fluorescence emission photons in the visible regime were coupled to a large-core step-index fiber with an outer diameter of 1 mm (Edmund Optics, Karlsruhe, Germany) and were remotely detected by a photomultiplier tube (PMT, RU5600, Hamamatsu, Japan) after passing a 2-mm BG39 emission filter (AHF Analysentechnik, Tübingen, Germany). The analog PMT current-signal was amplified by a variable gain current amplifier (Femto Messtechnik GmbH, Berlin, Germany) and digitized at 12 bits at 8-10 MHz with a multifunction data acquisition board (PCI-6115, National Instruments, TX).

For image generation the sampled fluorescence intensity values were assigned to their corresponding pixels based on a static lookup-table (LUT). Figure 1(e) (left) shows a two-photon image of 10-micron fluorescent microspheres obtained with the fiberscope. Individual microspheres are clearly discernible but image distortions (e.g., angular lag and pin-cushion distortions) are noticeable near the center of the image. These distortions were caused by phase and amplitude deviations of the actual fiber cantilever motion from the "ideal" trajectory defined by the drive signals. This effect is illustrated in Figure 1(d) for a small number of spiral lines. The distortions of the scan trajectory could be compensated for by applying a remapping-LUT [32] based on direct measurement of the actual cantilever motion using a 2D position-sensitive detector (S5991, Hamamatsu). Figure 1(e) (right) shows the image of 10-micron microspheres with a previously measured LUT applied. After remapping, microspheres had similar diameters near the center and at the periphery of the FOV and only minimal distortions remained in the center, which were only noticeable when slowly moving the FOV laterally. For functional imaging from specific cellular structures, correction of image distortions is optional.
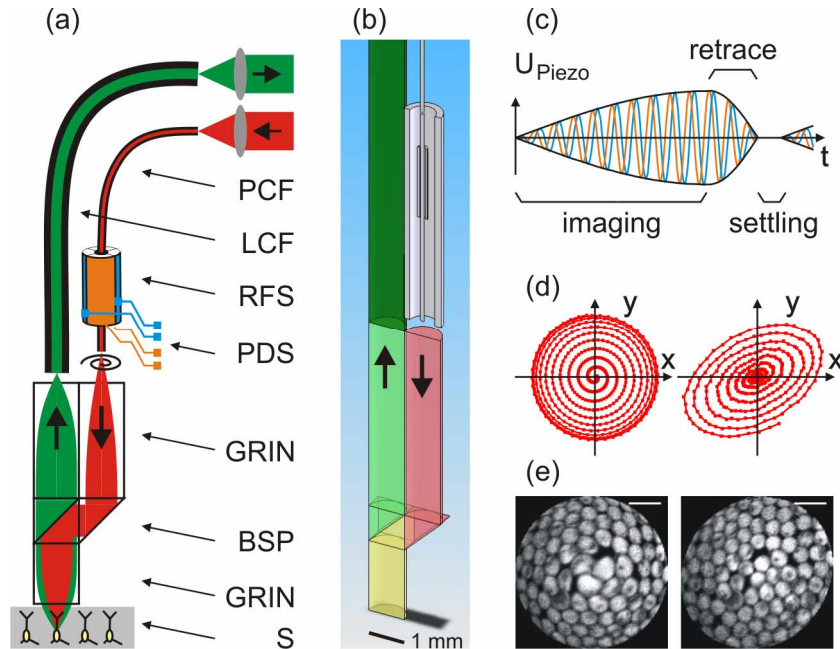
Fig. 1. Schematic (a) and perspective (b) representations of the ultra-compact fiber-optic two-photon microscope. A hollow-core PCF guides near-IR ultrafast laser pulses (red) to the microscope headpiece. The fiber cantilever is scanned in a spiral pattern by applying appropriate piezo drive signals (PDS) to a resonant fiber scanner (RFS). The motion of the fiber cantilever is imaged onto the sample (S) by a custom-designed combination of GRIN-lenses and micro-beamsplitter prisms (BSP). Fluorescence emission light (green) passes the GRIN objective lens and the BSP, is guided through a large core fiber (LCF) and detected by a photomultiplier tube. All optical components in the headpiece have millimeter dimensions. (c) Piezo drive signals for *x*- (blue trace) and *y*-direction (orange trace; 90° phase shifted). Amplitude modulation is used to create the spiral pattern. (d) 'Ideal' (left) and measured (right) scan trajectories, exemplified for a very small number of spiral lines. (e) Two-photon fiberscope images of 10-micron diameter fluorescent microspheres using an ideal (left) and a measured (right) scan trajectory for image reconstruction, respectively. Average laser power levels of 1 mW and 10x averaging were used. Scale bars are 20 µm.

Scan signal generation, data acquisition, and image reconstruction were controlled by a software package custom-written in the LabVIEW-environment (National Instruments, TX). Due to the compactness of the ultra-thin fiber scanner and the 1-mm dimension of the optical components, the total weight of the fiberscope headpiece was only 0.6 grams.

2.2 Characterization of spatial resolution

Functional imaging of cellular and subcellular activity requires micrometer spatial resolution. We therefore characterized the spatial resolution of the two-photon fiberscope by imaging subresolution (500-nm diameter) fluorescent microspheres at different positions throughout the FOV (Fig. 2(a)). Focusing was achieved by attaching the fiberscope headpiece to a micromanipulator. We analyzed the widths of the fluorescence intensity profiles along the lateral and axial directions (the contribution of the finite bead-sizes was estimated to be negligible, in the range of 3-4%). Specifically, intensity profiles were fitted with Gaussian-shaped distributions ($f(x) = y_0 + C \cdot \exp[-2 \cdot (x - x_0)^2/\sigma^2]$) to determine the lateral and axial standard deviations σ of the two-photon point-spread function (PSF) (Fig. 2(b) and (c)). The resulting σ-values were multiplied by a factor of $[2 \ln(2)]^{1/2}$ to obtain full-width-at-half-maximum (FWHM). The mean PSF-FWHM was 0.98 ± 0.09 µm laterally and 7.68 ± 1.30 µm axially (mean ± S.D., n = 10).

To translate the measured FWHM values to an "effective NA" we used a theory derived from Heisenberg's uncertainty principle [33]. For single-photon PSFs the lateral and axial FWHM values are given by [34]

$$\text{FWHM}_{\text{1p, lat}} = \frac{\lambda_0}{n\sqrt{3 - 2\cos(\alpha) - \cos(2\alpha)}} \tag{1}$$

$$\text{FWHM}_{\text{1p, ax}} = \frac{\lambda_0}{n\left[1 - \cos(\alpha)\right]} \tag{2}$$

where λ_0 is the vacuum wavelength, n the refractive index of the immersion medium, and α the half opening angle of the lens (NA = $n\sin(\alpha)$). The widths of the theoretical two-photon PSF were calculated according to $\text{FWHM}_{2p} = \text{FWHM}_{1p}\ 2^{-1/2}$ assuming Gaussian intensity distributions. Eqs. 1 and 2 were numerically solved for α following insertion of the experimentally determined FWHM values. The resultant effective NAs were 0.34 ± 0.03 and 0.38 ± 0.03 for the lateral and axial direction, respectively (Fig. 2(d)). Therefore the Gaussian-shaped beam emerging from the PCF nearly filled the back aperture of the front GRIN-lens. We conclude that the two-photon fiberscope provides micrometer resolution and thus should be well suited for imaging activity of cellular structures.
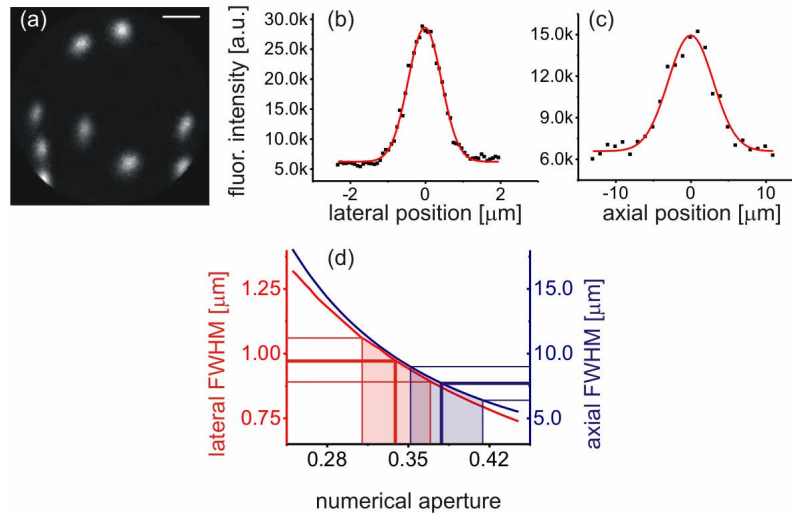
Fig. 2. Micrometer resolution of the two-photon fiberscope. (a) Two-photon image of 500-nm fluorescent microspheres. Scale bar 3 μm. Fluorescence intensity profiles of an example microsphere along the lateral (b) and the axial (c) dimension. Red traces are Gaussian-shaped curves fitted to the data points. (d) Calculation of the effective NA from the observed lateral (left, red) and axial (right, blue) FWHM. Horizontal lines represent mean ± S.D. The shaded areas correspond to the estimated error ranges of the calculated NAs in lateral and axial direction, respectively. Average laser power levels of 25 mW and 3x averaging were used.

2.3 Calcium measurements in rat cerebellum in vivo

To demonstrate the suitability of the ultra-compact two-photon fiberscope for functional measurements of neural activity, we applied the fiberscope to measure dendritic calcium signals in Purkinje cells of the rat cerebellum *in vivo*. All experiments were carried out according to the guidelines of the Institute for Laboratory Animal Science of the University Zurich, Switzerland and were approved by the Cantonal Veterinary Office. Long Evans rats (43-49 days old) were anesthetized by an intraperitoneal injection of urethane (1.5 g/kg body weight). A craniotomy was performed above cerebellum as previously described [35]. The dura was carefully removed and the exposed brain surface was superfused with normal rat

Ringer (NRR) solution (in mM: 135 NaCl, 5.4 KCl, 5 HEPES, 1.8 CaCl$_2$, pH 7.2 with NaOH). Population staining with the fluorescent calcium indicator Oregon Green-BAPTA 1 (OGB-1) was performed using the multi-cell bolus loading (MCBL) technique [35, 36]. Briefly, 50 µg of OGB-1 (acetoxymethyl(AM)-ester form; Molecular Probes, CA) were dissolved in 20% Pluronic F-127 (BASF, Florham Park, NJ) in DMSO and diluted in NRR to a final concentration of 1 mM. This solution was pressure injected directly into the molecular layer of cerebellar cortex, about 100-150 µm below the surface. Within one hour, MCBL unspecifically stained various cellular components in the molecular layer including dendrites of Purkinje neurons [35, 37].

The fiberscope headpiece was lowered onto the surface of the exposed cerebellum without penetrating the tissue. Time-lapse imaging was performed in the upper molecular layer at effective frame rates of 7-15 fps (2-3 frames averaged) and with ~150-200 mW laser power at the sample. We observed spontaneous fluorescence intensity fluctuations in parasagittal stripes, reminiscent of previously reported calcium signals in Purkinje cell dendrites [35, 37] (Fig. 3(a)). These calcium signals were expressed as relative fluorescence intensity changes (ΔF/F) after background subtraction. Gaussian blurring was used to remove shot noise from the PMT. Pseudocolor-coded movies of fluorescence changes were subsequently rendered in ImageJ (NIH, MD) by merging the time series of ΔF/F images (as hue H and saturation S) with the average fluorescence image (as brightness B) into a single HSB-movie (Fig. 3(a)).
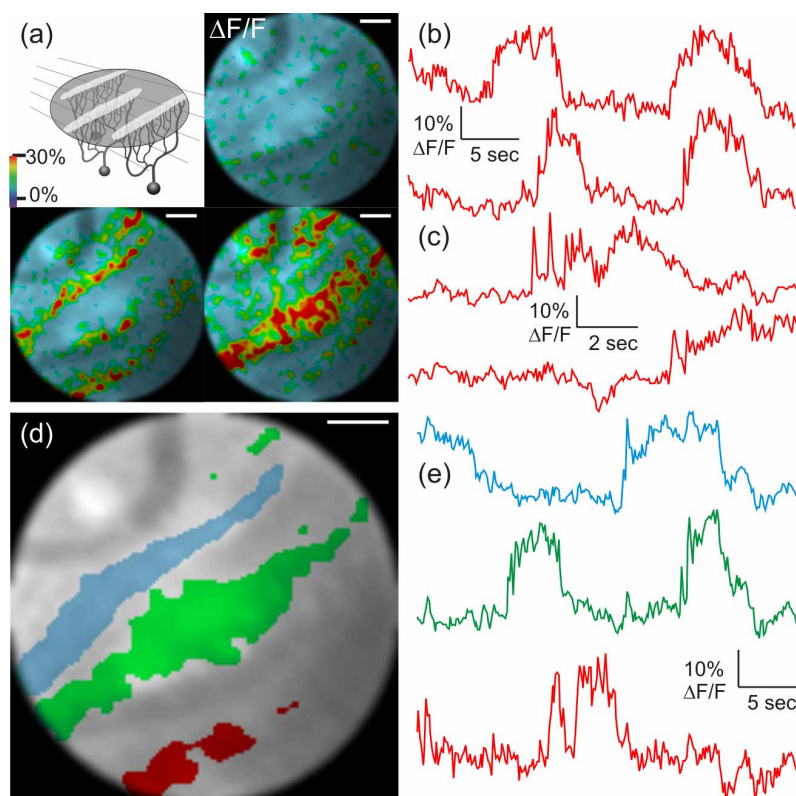

Fig. 3. (a) The cerebellar cortex has a well-defined anatomical organization with flat dendritic trees of Purkinje cells lying in parasagittal planes. In top view, dendritic excitation is evident as band-like calcium signals. Three snapshots from a ΔF/F movie of 33 s total duration are provided. (b and c) Examples of spontaneous ΔF/F-traces in ROIs comprising different dendrites. Note the different time scales. (d) Example of semi-automated ROI-definition by ICA. (e) Corresponding ΔF/F-traces color-coded according to the ROI selections in (d). All scale bars are 15 µm.

The time course of calcium signals was analyzed in regions of interest (ROIs) corresponding to putative Purkinje cell dendrites. Due to the weak contrast between background and dendritic structures we used a semi-automated procedure for ROI-selection. The algorithm is based on independent component analysis (ICA, JADE, [38]), which blindly separates signals from different sources. Effectively, pixels with a time course similar to a particular signal source (based on correlation analysis) were grouped into separate ROIs (Fig. 3(d)). In 4 animals, we found brief calcium transients in putative Purkinje cell dendrites overlaid on top of slower calcium oscillations (Fig. 3(b), (c), and (e)). Signal amplitudes and noise levels were comparable to standard two-photon imaging studies. The fast signals were characterized by 10-25% $\Delta F/F$ amplitudes and an average decay time constant of $\tau = 0.20 \pm 0.08$ s (mean $\pm$ S.D., n = 15). Slow oscillations typically lasted 5–8 seconds and occurred every 10-15 seconds. These findings are in agreement with previous *in vivo* imaging studies on Purkinje neurons [35, 37].

4. Discussion

By combining the – to our knowledge – best technologies from different fields (PCF for efficient femtosecond pulse delivery, miniaturized spiral scan engine for beam steering, GRIN-optics for focusing and beam-splitting), we introduced an ultra-compact, highly sensitive two-photon excitation fluorescence microscope which promises to enable neural network dynamics studies in freely behaving animals. In contrast to previous Lissajous-pattern-based fiber-scanners (e.g., [11, 23]), our spiral scanner does not rely on an additional stiffening piece on the fiber for breaking spatial symmetry and creating two different resonance frequencies. Therefore the spiral scanner can be designed ultra-thin with outer diameters as small as 1 mm. Phase- and amplitude-deviations in spiral scanners can be compensated by empirical radius-dependent angular lag functions [24] or – as shown here – by experimentally determined scan-trajectories. Alternative scanning approaches such as MEMS-based scan engines [27, 28] and "piezolever" fiber scanners [26], enable galvanometric-like beam-steering and random-access scanning albeit at the cost of slower scan speeds and expensive, time-consuming manufacturing processes. Finally, imaging through coherent fiber bundles suffers from reduced spatial resolution [19, 30].

Our fiberscope could be further improved in several ways. First, in the current design, pixel dwell times become shorter with increasing spiral radius because fiber velocities are higher at the periphery. As a consequence, image brightness levels are reduced in the outer part of the images. Modulation of the analog gain with radial position may improve image homogeneity, although it leads to increased noise levels in the periphery. A different compensation mechanism is laser power modulation. However, changing laser power typically affects the resonance properties of the fiber cantilever due to thermal heating. Therefore, a second improvement would be to incorporate a temperature stabilization unit into the spiral scanner. However, brightness normalization is not essential for recording relative fluorescence changes ($\Delta F/F$). As a third improvement a focusing mechanism could be included in the fiberscope headpiece. At present, our microscope is designed for imaging in a fixed two-dimensional plane. Studies on freely moving animals will therefore require positioning and subsequent fixation of the microscope headpiece. If recordings from different optical sections are required during the experiment, remote focusing can be achieved with a miniature DC motor, which adds only little weight [11, 23]. Most simply, adjustment of the distance between the GRIN tube lens and the fiber scanner can be used to axially shift the focal plane.

Most *in vivo* two-photon imaging studies have used anesthetized animals. However, correlation of neuronal network activity with behavior is not possible during anesthesia. Two principal approaches may extend functional two-photon microscopy to awake preparations: head-restraint animals [39] and head-mounted microscopes [11]. The first approach benefits from the use of conventional two-photon microscopes providing good image quality but may be applicable to a limited set of behavioral paradigms only. The second approach, for which our two-photon fiberscope is designed, promises to enable a wider range of behavioral studies

at the cost of slightly deteriorated image quality. Thus, complementary results can be expected from these different approaches. Fiberscope imaging in unrestrained animals promises comprehensive insights into neural network activity and its correlation to specific behaviors. Fields of applications include the functional studies of neocortex, cerebellum and other superficial brain areas as well as endoscopic targeting of subcortical regions [9, 10, 18]. Finally, clinical applications comprising medical imaging and treatment can be envisioned.

5. Conclusion

We have presented a novel ultra-compact two-photon microscope for functional calcium imaging *in vivo*. Our device is based on miniaturized components for beam steering and epifluorescence detection. The headpiece weighs only 0.6 grams and should be easily portable by a rat or a mouse. Spatial resolution is ~1 μm. Fluorescence collection sensitivity and achievable frame rates are sufficient for reliable recordings of functional calcium transients. We conclude that our fiberscope will be well suited for optical recording of neural network dynamics in awake, freely behaving animals.

Acknowledgments